


# Effects of $\pi^*$ - $\sigma^*$ coupling on dissociative-electron-attachment angular distributions in vinyl, allyl, and benzyl chloride and in chlorobenzene

Pamir Nag <sup>\*</sup>, Michal Tarana <sup>†</sup>, and Juraj Fedor <sup>‡</sup>

*J. Heyrovský Institute of Physical Chemistry, Czech Academy of Sciences, Dolejškova 3, 18223 Prague, Czech Republic*

 (Received 29 January 2021; accepted 12 March 2021; published 29 March 2021)

We report on a velocity map imaging study of  $\text{Cl}^-$  anions resulting from the dissociative electron attachment to four unsaturated chlorohydrocarbons. In all four molecules, this process is mediated by the formation of the lowest shape resonance. The choice of the molecules was motivated by the different character of this resonance. In the planar compounds chlorobenzene and vinyl chloride, it is a  $\pi^*$  resonance, which is not dissociative along the C-Cl bond without distortion of the planar geometry. In the nonplanar compounds benzyl chloride and allyl chloride, the shape resonance has a mixed  $\pi^*$ - $\sigma^*$  character and is directly dissociative without the need for any additional distortion. Our motivation was to find out whether the dissociation-allowing nuclear motion has a common imprint in the resulting fragment angular distributions. In spite of the expected similarities between the two classes of compounds, the resulting images are quite different for all four molecules. We interpret the results, especially the imprints of the bending dynamics, with the aid of a single-electronic-state model in the axial recoil approximation.

DOI: [10.1103/PhysRevA.103.032830](https://doi.org/10.1103/PhysRevA.103.032830)

## I. INTRODUCTION

Dissociative electron attachment (DEA) is a mechanism that mediates molecular bond-cleavage and is ubiquitous in many diverse environments, including plasmas, biological tissue during passage of high-energy radiation, or focused-beam nanofabrication [1]. It is interesting also from a purely fundamental point of view of nuclear dynamics: the DEA is mediated by the formation of resonances—transient anions—which have an autodetachment lifetime often on a timescale comparable to that of the nuclear motion during the bond cleavage. This is especially true for shape resonances where the incoming electron interacts with the ground electronic state of the target molecule (the core-excited resonances are typically much narrower with a long autodetachment lifetime [2]). The electronic width of a shape resonance depends on the angular momentum of the trapped electron since that determines the barrier toward the electron detachment. Typically,  $\sigma^*$  resonances are extremely broad, which results in very fast autodetachment, whereas  $\pi^*$  resonances are narrower and in some cases give rise to very high DEA cross sections.

There is an interesting class of molecules where a  $\pi^*$  resonance is formed; however, due to symmetry constraints, the anion cannot dissociate without a geometry distortion. This was first pointed out in a beautiful classic paper by Clarke and Coulson [3], who, using only symmetry arguments, constructed potential energy curves in chlorobenzene. The DEA in this molecule yields  $\text{Cl}^-$  and phenyl radical in their ground electronic states. At the same time, the  $\pi^*(b_1)$  resonance

(later found to be centered around 0.75 eV [4,5]) cannot yield these fragments upon mere stretching of the C-Cl bond because it does not correlate asymptotically with the product electronic states. Rather, upon geometry distortion during the dissociation—most probably out-of-plane motion of the Cl atom—the  $\pi^*$  state mixes with the  $\sigma^*(\text{C-Cl})$  state and opens the dissociation pathway. Burrow and co-workers [6] were the first to realize that in benzyl chloride, where the Cl atom is positioned out of plane in the equilibrium geometry and the planar symmetry is absent, the corresponding resonance has mixed  $\pi^*$ - $\sigma^*$  symmetry, and the dissociation pathway is directly open. Indeed, they measured that the dissociative cross section in benzyl chloride is higher by a factor of 17.5 than in chlorobenzene (the direct pathway means a shorter dissociation time, and fewer anions decay by autodetachment). The same symmetry situation arises in the pair vinyl chloride, where the Cl atom is in the molecular plane, versus allyl chloride, where the C-Cl bond points out-of-plane. Again, the DEA cross section in the latter is larger than that in the former by a factor of 5.3.

This pioneering work inspired a large amount of research. On the one hand, this concerned electron collisions with unsaturated chlorinated compounds. The resonance positions (vertical attachment energies) in the four molecules in question were further refined by electron transmission spectroscopy [4,7]. The DEA spectra were also measured by several groups [4,7,8]. Skalicky *et al.* [5] probed vibrational excitation of chlorobenzene by electron energy loss spectroscopy and pointed out that the out-of-plane C-Cl motion is not the only vibration that opens the DEA pathway, and that other ring distortions can also play a role. The electron attachment rates of all four compounds were measured in various swarm experiments [9–11]. Theoretically, the resonances in chlorobenzene were explored by scattering calculations [12].

<sup>\*</sup>pamir.nag@jh-inst.cas.cz

<sup>†</sup>michal.tarana@jh-inst.cas.cz

<sup>‡</sup>juraj.fedor@jh-inst.cas.cz

The interest was of course not limited to chlorinated compounds. The problem of symmetry lowering in DEA attracted a lot of attention in general, both experimentally and theoretically. The instructive examples from organic compounds are acetylene [13,14], HCN [15,16], formic acid [17–19], methyl formate [20], or HNCO [21].

In this paper, we address this problem using the velocity map imaging (VMI) technique. Since the introduction of DEA VMI by Krishnakumar and co-workers some 15 years ago [22], the fragment angular distributions directly provided by this technique shed a lot of light on many problems of DEA nuclear dynamics. Our choice of target systems was directly inspired by the original paper of Burrow and co-workers [6]: chlorobenzene and vinyl chloride are planar and require distortion to allow DEA, while in benzyl- and allyl-chloride the DEA can proceed simply by C-Cl bond stretching. We question whether this fact leads to common imprints in the fragment images. As will be seen, the answer is no.

## II. EXPERIMENTAL SETUP

A DEA cross-section measurement setup [14,23] was modified recently to measure the angular and kinetic energy distribution of anionic fragments using the velocity map imaging technique [24,25]. Details of the experimental setup can be found elsewhere [26]. The experiments are performed under high vacuum condition with a base pressure around  $\sim 10^{-8}$  mbar. A magnetically collimated pulsed electron beam produced using a trochoid electron monochromator [27] is made to interact perpendicularly with an effusive molecular beam. The pulsed electron beam is of 300-ns width and generated at a 40-kHz repetition rate.

A time- and position-sensitive detector with a 40-mm active diameter is used in the experimental setup. The detector consists of a pair of microchannel plates (MCPs) in a chevron configuration, placed at about 5 mm away from the drift tube, and an LC delay-line hexanode [28], placed outside of the vacuum chamber. Two different sets of data acquisition systems were used for velocity map imaging and ion-yield measurement purposes. The  $x$ - $y$  position of each detected ion was measured from the three pairs of delay-line signals from the hexanode, whereas only the MCP signal was used for the ion-yield curve measurement purpose. The *velocity map imaging* condition ensures that all the ions created with the same momentum at different positions reach the detector at the same point. The angular distribution of the anions was obtained from central sliced images, whereas the information about the kinetic energy distribution was obtained from the half-“Newton sphere” [26].

The incident electron beam current in pulsed mode was around 350 pA during the measurements. The electron beam energy scale was calibrated using the 4.4-eV resonance peak of  $\text{O}^-/\text{CO}_2$ , and the electron beam energy resolution was around 350 meV. The background pressure in the chamber during the measurements was  $\sim 2 \times 10^{-6}$  mbar. The single collision condition was verified by the linear signal dependence on the sample pressure. The current measurements were complicated by the fact that the presence of chlorinated molecules was strongly shifting the energy scale calibration during the measurements (probably by influencing the

contact potentials of the monochromator electrodes). We tried to minimize the systematic errors in incident energy by repeated calibration with  $\text{CO}_2$  before and after taking each dataset. The uncertainty in the energy position of the anion yields is thus in the order of the electron energy resolution ( $\pm 150$  meV). All velocity map images presented here are the result of a single measurement, without any summation or averaging of data sets.

During measurements, all the four samples were kept in a heat-bath at a constant temperature of 23 °C, and except for vinyl chloride, all the samples are liquid at room temperature. All four samples were commercially purchased from Sigma-Aldrich and had different levels of purity. The allyl chloride sample used for the experiment was 99% pure assay. For the experiments with chlorobenzene, a 99.8% pure anhydrous sample was used, and for benzyl chloride a 99% pure assay with <1% propylene oxide as stabilizer was used. A 2000- $\mu\text{g}/\text{mL}$  solution of vinyl chloride in methanol was used for the experiments with vinyl chloride. Since we only detect chlorine anions, we presume that the possible presence of the solvent molecules in the target vapor did not influence the spectra. To remove any solvated gas from the samples (except for vinyl chloride), a few cycles of freeze-thaw and pump were performed before the experiments.

## III. THEORY

A theory that relates the symmetry of the electronic resonance with the angular distribution of the anionic fragments in the DEA was developed by O’Malley and Taylor [29]. It was formulated for the diatomic targets and based on the assumptions that only a single resonance is involved in the DEA. The coupling is due to a pure electronic matrix element (independent of spin), and the fact that the negative ion does not rotate during the dissociation (axial recoil approximation).

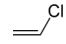

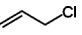
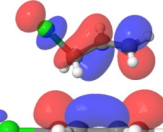
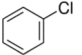
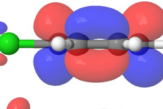
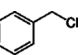
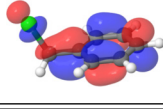
Azria *et al.* [30] later generalized this theory to treat the polyatomic molecules using the same approximations. That yielded the following expression for the intensity of the anionic fragments  $I$  as a function of the angle  $\vartheta$  with respect to the incoming electron beam:

$$I^\epsilon(\vartheta) \propto \frac{1}{2\pi} \int_0^{2\pi} \left| \sum_{lm} a_{lm} i^l e^{i\delta_l} X_{lm}^\epsilon(\vartheta, \varphi) \right|^2 d\varphi, \quad (1)$$

where  $\vartheta$  and  $\varphi$  are the polar angles of the electron beam in the dissociation frame, and  $X_{lm}^\epsilon(\vartheta, \varphi)$  are the basis functions for the irreducible representations of the point group  $G$  of the molecule also expressed in the dissociation frame. The expansion coefficients  $a_{lm}$  are real, and the phases  $\delta_l$  represent a contribution of the direct scattering to the electronic part of the process [31]. The values of the indices  $l$  and  $m$  with a nonzero contribution to the sum in Eq. (1) are restricted by the irreducible representation of the electronic resonant state  $\epsilon$ .

This theory was previously successfully utilized to interpret several experimentally obtained angular spectra of the DEA for several diatomic [31] and polyatomic molecules [30,32–34]. The values of  $a_{lm}$  fitted to the experimental spectra revealed the relative contributions of different symmetries

TABLE I. Properties of target molecules used in the present study. The details are provided in the main text.

Name	Structure	LUMO (Present)	Resonance type Refs. [4,7]	$E_{\text{res}}$ (eV) Refs. [4,7]	$E_{\text{th}}$ (eV) (Present)	DEA peak (eV) (Present)
Vinyl chloride			$\pi^*(a'')$	1.28	0.065	1.3
Allyl chloride			$\pi^*/\sigma_{\text{C-Cl}}^*$	1.01	-1.07	0.8 eV
Chlorobenzene			$\pi^*(b_1)$	0.75	0.150	0.7 eV
Benzyl chloride			$\pi^*/\sigma_{\text{C-Cl}}^*(a')$	0.64	-0.94	0.8 eV

of the scattering system and partial waves of the colliding electron to the DEA.

Although the coupling of two resonances cannot be properly treated by the model of Azria *et al.* [30], its application to the systems studied in this work still provides a valuable insight into the underlying mechanisms. The significance of the  $\pi^*$  state mixing with the  $\sigma^*$  state can be assessed by the differences between the measured angular distributions and those provided by Eq. (1) for the electron capture into the  $\pi^*$  state.

At this point, it is worth mentioning that the basis functions  $X_{lm}^\epsilon(\vartheta, \varphi)$  in Eq. (1) are generally constructed in two steps: First, the basis set for the irreducible representation is expressed in terms of the spherical harmonics in the body frame where the  $z$ -axis coincides with the symmetry axis of the molecule. Subsequently, these functions are expressed in a coordinate system rotated in such way that its  $z$ -axis coincides with the direction of the dissociation; a corresponding transformation is performed in terms of the Wigner  $D$  matrices [35]. Note that this rotation is not necessary for any molecule discussed in this work. The symmetry axis of chlorobenzene coincides with the dissociating C-Cl bond. The symmetry point group of the remaining three molecules  $C_s$  does not possess any symmetry axis. Therefore, the  $z$ -axis oriented along the C-Cl bond does not violate the symmetry. It simultaneously allows for an evaluation of  $X_{lm}^\epsilon(\vartheta, \varphi)$  in the dissociation frame without any additional rotation.

## IV. RESULTS AND DISCUSSION

### A. Energetics, ion yields, and kinetic energy distributions

Table I lists the relevant properties of the four target molecules in this study: the structure, the isosurface of the lowest unoccupied molecular orbital [HF/6-31G(d) level], the resonance energy  $E_{\text{res}}$  corresponding to the temporal occupation of this orbital, the DEA threshold energy  $E_{\text{th}}$ , and the DEA peak energy. The resonance energies are taken from the literature. There is a certain scatter of values from various electron transmission experiments [4,6,7,36,37], however the scatter is in the order of 100 meV, not influencing any present

conclusions. For the sake of consistency, we tabulate the most recent ETS resonance energies from the group of Modelli [4,7]. The DEA threshold energies  $E_{\text{th}}$  (the lowest energies at which the  $\text{Cl}^-$  production is energetically allowed) were calculated at the B3LYP/aug-cc-pVDZ level as the energy difference between the reactants and products, including the zero point energies. The positive values mean that the DEA reaction is endothermic, while the negative values mean that the reaction is exothermic and could in principle proceed even at zero electron energy [38]. As will be seen, it does not proceed at zero energy; the fragments appear only at resonance energies.

The kinetic energy released after the dissociation due to electron attachment will be distributed among the neutral and the anionic fragments. If  $E_{\text{in}}$  is the energy of the incident electron, then by using energy and momentum conservation, the kinetic energy of the anionic fragment  $E_{\text{ke}}$  can be expressed as

$$E_{\text{ke}} = \left(1 - \frac{m}{M}\right)[E_{\text{in}} - (E_{\text{th}} + E^*)], \quad (2)$$

where  $m$  ( $= 35.453$  amu) and  $M$  are the masses of the  $\text{Cl}^-$  fragment and the parent molecule, respectively. The  $M$  for vinyl chloride, allyl chloride, chlorobenzene, and benzyl chloride are considered to be 76.53, 62.498, 112.56, and 126.58 amu.  $E^*$  is the energy going to the internal degrees of freedom of the neutral fragment. The maximum kinetic energy that the  $\text{Cl}^-$  fragment can carry is for  $E^* = 0$ , when all the excess energy is released from of the kinetic energy.

Figures 1–4 show the present results. In all four figures, panel (a) shows the  $\text{Cl}^-$  ion yield. Each compound shows one isolated DEA peak. For each molecule, we have measured the  $\text{Cl}^-$  velocity map images (3D Newton spheres) at several electron incident energies across its peak. The central slices are shown in panels (e)–(g) [(d)–(f) for chlorobenzene]. Panels (b) show the corresponding kinetic energy distributions of the  $\text{Cl}^-$  fragment, evaluated from the forward Newton half-spheres as described in Ref. [26]. Panels (c) show the angular distributions of fragments. The only exception is chlorobenzene (Fig. 4), which shows near-isotropic angular distributions.

The current ion yields are in good agreement with the previous reports [4,6,7,39,40]. As to the kinetic energy

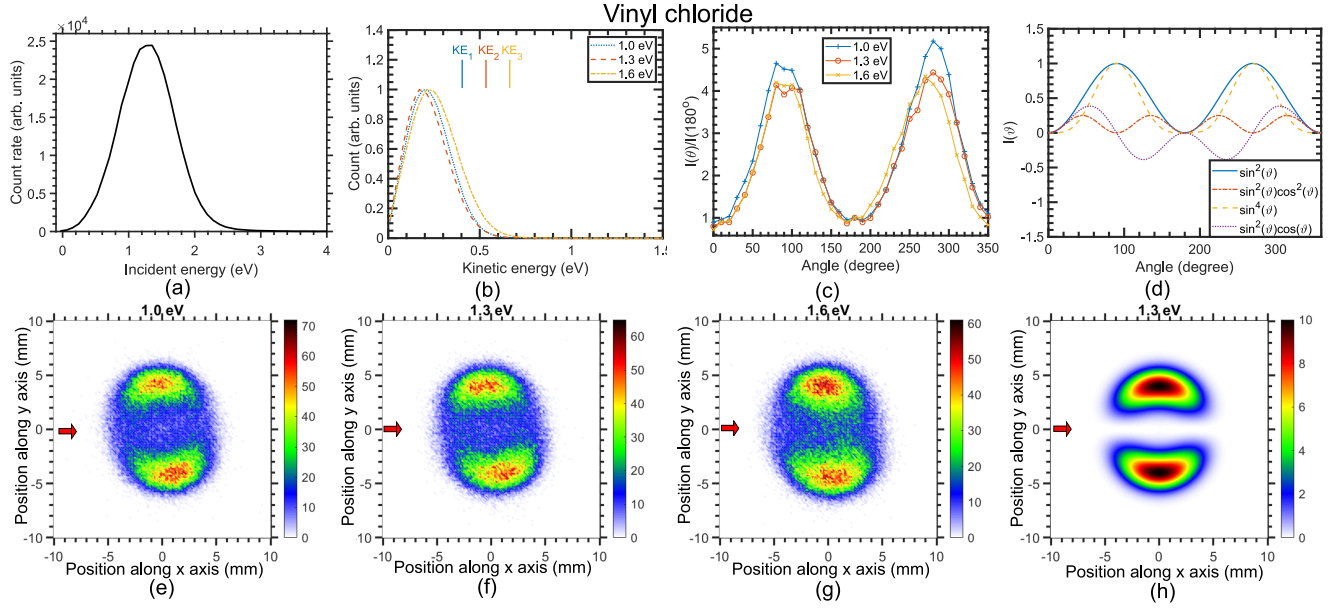


FIG. 1. The results for vinyl chloride. (a) The  $\text{Cl}^-$  ion yield as a function of the incident electron energy. (b) The kinetic energy distributions of  $\text{Cl}^-$  for three different incident energies. (c) The angular distribution of the  $\text{Cl}^-$  ions for these energies. (d) Individual angular terms from Eq. (4). (e),(f),(g) The velocity map images of  $\text{Cl}^-$  (central time slices) at three different incident energies. The incident electron beam is depicted by red arrows. (h) Simulated image using the experimental KER at the incident energy of 1.3 eV and the  $\sin^2 \vartheta$  angular distribution (pure  $p$ -wave).

distributions (given by the radial extent of the fragments on the images), in all four target molecules they show a surprisingly small dependence on the incident electron energy. To illustrate this, we added vertical bars in all panels (b) which show the maximum  $\text{Cl}^-$  kinetic energies if all the excess energy went into translation ( $E^* = 0$ ). These shift considerably to the right with increasing energy, while the measured kinetic energy distributions are almost unchanged. In a few cases, the measured distribution has a tail extending to higher energies than the calculated maximum; this is an effect of the instrumental resolution.

The most puzzling result are the angular distributions. They are considerably different in all four cases. Before discussing them one by one, we note that for all the images of all the target molecules there should be an axial symmetry around the  $x$ -axis since the kinematics has to be cylindrically symmetric around the incident beam direction. The weak deviations from this symmetry are caused by the presence of the magnetic field and are explained in detail in Ref. [26].

### B. Angular distributions: Vinyl chloride

The experiment shows that most fragments in vinyl chloride leave the collision in the perpendicular direction to the electron beam. The symmetry point group of the planar target molecule is  $C_s$ . The  $a''(\pi^*)$  resonance is antisymmetric with respect to the molecular plane.

It is not dissociative upon mere C-Cl stretching and without out-of-plane geometry distortion. Nonetheless, it is instructive to calculate the angular distribution in the approximation that disregards any distortion. The difference between this model

and the experimental data can then be attributed to the effect of bending nuclear dynamics.

Using the coordinate system introduced in Sec. III, where the  $z$ -axis is oriented along the C-Cl bond and the  $xz$  plane coincides with the molecular plane, the basis functions of the irreducible representation  $a''$  can be expressed as

$$X_{lm}^{a''}(\vartheta, \varphi) = \frac{1}{\sqrt{2}i} [Y_l^m(\vartheta, \varphi) - (-1)^m Y_l^{-m}(\vartheta, \varphi)] \\ = N_{lm} P_{lm}(\cos \vartheta) \sin(m\varphi), \quad (3)$$

where  $l, m > 0$ ,  $Y_l^m(\vartheta, \varphi)$  are the spherical harmonics [35],  $P_{lm}(x)$  are the associated Legendre polynomials, and  $N_{lm}$  are the real normalization factors.

Restriction of the sum in Eq. (1) to the two lowest partial waves  $p$  and  $d$  that have a nonzero contribution to  $I^{a''}(\vartheta)$  yields

$$I^{a''}(\vartheta) = \alpha_{11}^2 \sin^2 \vartheta + \alpha_{21}^2 \sin^2 \vartheta \cos^2 \vartheta + \alpha_{22}^2 \sin^4 \vartheta \\ + 2\alpha_{11}\alpha_{21} \sin(\delta_1 - \delta_2) \sin^2 \vartheta \cos \vartheta, \quad (4)$$

where  $\alpha_{lm}$  are rescaled coefficients  $a_{lm}$  to absorb the constant factors. The terms in the first row represent the contributions from the individual partial waves. The last term in the second row is due to a mixing between the partial waves  $p$  and  $d$ .

Figure 1(d) shows the individual terms of Eq. (4). The lowest partial wave with nonzero contribution ( $p$ -wave) has the angular distribution of  $\sin^2 \vartheta$ . It is worth noting that in a diatomic-like model where only the symmetry of the breaking C-Cl bond would be considered, a resonance with  $\pi^*$  symmetry with respect to this bond would have the same angular distribution [29]. Interestingly, this contribution itself explains the experimental data very well. To demonstrate it



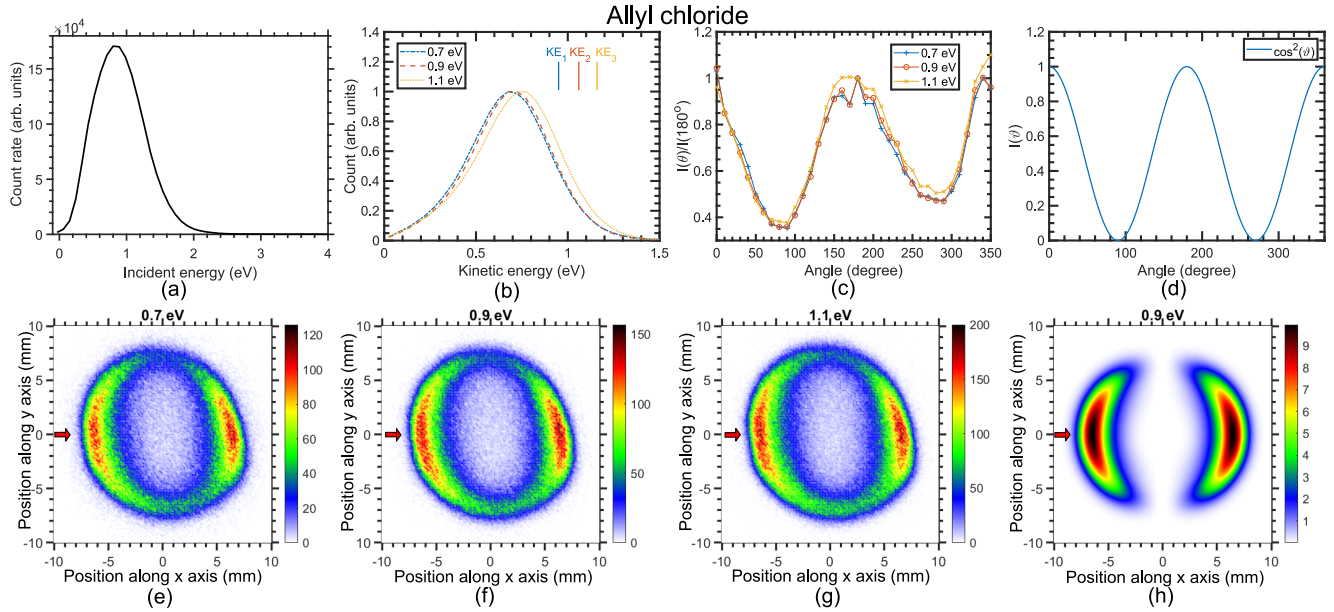


FIG. 2. The results for allyl chloride. (a) The  $\text{Cl}^-$  ion yield as a function of the incident electron energy. (b) The kinetic energy distributions of  $\text{Cl}^-$  for three different incident energies. (c) The angular distribution of the  $\text{Cl}^-$  ions for these energies. (d) Angular term from Eq. (5). (e),(f),(g) The velocity map images of  $\text{Cl}^-$  (central time slices) at three different incident energies. The incident electron beam is depicted by red arrows. (h) Simulated image using the experimental KER at the incident energy of 0.9 eV and the  $\cos^2 \vartheta$  angular distribution.

graphically, we have generated a hypothetical VMI image [Fig. 1(h)], for which we used the experimental KER and the theoretical angular profile  $\sin^2 \vartheta$ . The very good agreement with the observed distribution means that the deviation of the C-Cl bond from the planar geometry during the dissociation has to be very small since it does not visibly influence the resulting angular distribution.

### C. Angular distributions: Allyl chloride

As can be seen in Fig. 2, the measured DEA angular spectra of allyl chloride show maxima in forward and backward directions. This molecule does not possess any specific overall symmetry. Nevertheless, the diatomic-like model introduced in Sec. IV B, that considers only the symmetry of the breaking bond, still can be constructed. The symmetry of the C-Cl bond (when the rest of the molecule is disregarded) is  $\sigma^*$ . The basis set of the corresponding irreducible representation is  $X_{l0}^{\sigma^*}(\vartheta, \varphi) = Y_l^m(\vartheta, \varphi)$ . The lowest partial wave contributing to the angular intensity profile is  $l = 1, m = 0$ . This corresponds to the angular dependence

$$I^{\sigma^*}(\vartheta) = \alpha_{10} \cos^2 \vartheta. \quad (5)$$

This function is shown in Fig. 2(d). Again, we have generated a hypothetical VMI image using this angular distribution and the experimental KER [Fig. 2(h)]. The simple diatomic-like model taking into account only the  $\sigma^*$  character of the C-Cl bond thus reproduces the experimental distribution very well.

### D. Angular distributions: Chlorobenzene

The angular distributions of  $\text{Cl}^-$  for the DEA to chlorobenzene (Fig. 3) show central intensive blobs with weakly prolate shapes. The symmetry point group of this molecule is  $C_{2v}$ .

The electron is captured in a resonance with  $b_1$  symmetry. As in vinyl chloride, the C-Cl bond is not dissociative without an additional geometry distortion.

The basis of the irreducible representation  $b_1$  can be in the coordinate system with the  $z$ -axis along the C-Cl bond and with the  $yz$  plane coinciding with the molecular plane expressed as

$$\begin{aligned} X_{lm}^{b_1}(\vartheta, \varphi) &= \frac{1}{\sqrt{2}} [Y_l^m(\vartheta, \varphi) - Y_l^{-m}(\vartheta, \varphi)] \\ &= N_{lm} P_{lm}(\cos \vartheta) \cos(m\varphi), \end{aligned} \quad (6)$$

where  $l > 0$ , and  $m$  attains only odd positive values.

Assuming only the lowest partial waves  $p$  and  $d$  that have nonzero contribution to the sum in Eq. (1), the intensity  $I^{b_1}(\vartheta)$  can be expressed as follows:

$$\begin{aligned} I^{b_1}(\vartheta) &= \alpha_{11}^2 \sin^2 \vartheta + \alpha_{21}^2 \sin^2 \vartheta \cos^2 \vartheta \\ &\quad - 2\alpha_{11}\alpha_{21} \sin(\delta_2 - \delta_1) \sin^2 \vartheta \cos \vartheta, \end{aligned} \quad (7)$$

where  $\alpha_{lm}$  are the rescaled coefficients  $a_{lm}$  to absorb the constant prefactors. The individual contributions are the same as in allyl chloride. Taking into account only the lowest allowed partial wave ( $p$ ), the angular distribution goes as  $\sin^2 \vartheta$ , which is plotted in Fig. 3(c).

In this case, there is a clear disagreement of the experimental data with the one-state model. One should note that inclusion of higher partial waves from Eq. (7) would not solve this disagreement: all the angular contributions have zero value at  $0^\circ$  and  $180^\circ$  and they thus lead to a nodal line along the incident beam direction. The experimental distributions, however, have intensity maxima along this line. One should keep in mind that for such low values of energy release as in chlorobenzene, the thermal velocity spread of the target

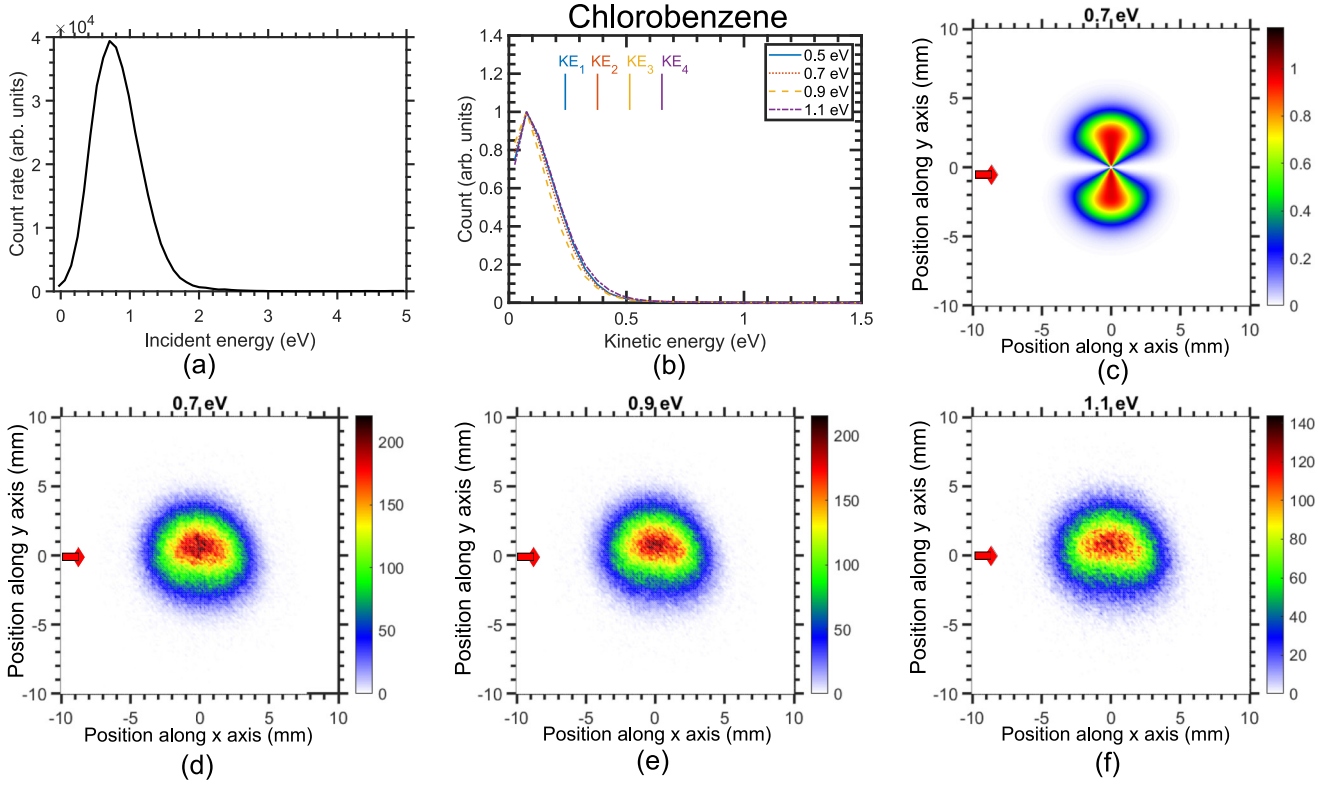


FIG. 3. The results for chlorobenzene. (a) The  $\text{Cl}^-$  ion yield as a function of the incident electron energy. (b) The kinetic energy distributions of  $\text{Cl}^-$  for four different incident energies. (c) Simulated image using the experimental KER at the incident energy of 0.7 eV and the  $\sin^2 \vartheta$  angular distribution. (d),(e),(f) The velocity map images of  $\text{Cl}^-$  (central time slices) at three different incident energies. The incident electron beam is depicted by red arrows.

molecules can considerably influence the resulting image. The mean thermal energy at 300 K is 39 meV. Combined with the resolution of the imaging system, this can lead to smearing of the signal over the central nodal line. Still, the prolate shapes of the experimental images suggest a component in the direction parallel to the electron beam. This might be caused by the bending dynamics of the transient anion, e.g., via the appearance of the  $\cos^2 \vartheta$  component due to the  $\sigma^*(\text{C-Cl})$  state as in allyl chloride.

### E. Angular distributions: Benzyl chloride

The experimental angular profiles for benzyl chloride plotted in Fig. 4 are perhaps the most peculiar. They show a weak preference for the perpendicular fragment direction, which is, however, not very pronounced. Perhaps more importantly, this is the only molecule where a clear forward-backward asymmetry is present. It also shows the seemingly strongest up-down asymmetry (artifact due to the presence of the magnetic field); this is, however, dictated by the large spacial spread of the Newton sphere on the detector. Allyl chloride, which has a similar spacial spread, shows a minimum intensity in the perpendicular direction, so there this effect is visible much more weakly. We have checked the reproducibility of the forward-backward asymmetry by recording the benzyl chloride images under different conditions (e.g., via deflecting the Newton sphere to different areas of the detector).

A symmetry plane of the target molecule is perpendicular on the ring and includes the C-Cl bond (point group  $C_s$ ). The lowest electronic resonance is symmetric with respect to the symmetry plane ( $a'$ ). Using the same coordinate system with respect to the symmetry plane as in vinyl chloride, the basis of the irreducible representation  $a'$  is

$$\begin{aligned} X_{lm}^{a'}(\vartheta, \varphi) &= \frac{1}{\sqrt{2(1 + \delta_{m0})}} [Y_l^m(\vartheta, \varphi) + (-1)^m Y_l^{-m}(\vartheta, \varphi)] \\ &= N_{lm} P_{lm}(\cos \vartheta) \cos(m\varphi), \end{aligned} \quad (8)$$

where  $l, m \geq 0$ .

Assuming only the partial waves  $s$ ,  $p$ , and  $d$ , the intensity  $I^{a'}(\vartheta)$  can be expressed using the rescaled coefficients  $\alpha_{lm}$  as follows:

$$\begin{aligned} I^{a'}(\vartheta) &= \alpha_{00}^2 - 2\alpha_{00}\alpha_{10} \sin(\delta_1 - \delta_0) \\ &\quad + \alpha_{10}^2 \cos^2 \vartheta + \alpha_{11}^2 \sin^2 \vartheta + \alpha_{20}^2 (3 \cos^2 \vartheta - 1)^2 \\ &\quad + \alpha_{21}^2 \cos^2 \vartheta \sin^2 \vartheta + \alpha_{22}^2 \sin^4 \vartheta \\ &\quad - 2\alpha_{00}\alpha_{20} \cos(\delta_2 - \delta_0) (3 \cos^2 \vartheta - 1) \\ &\quad - 2\alpha_{10}\alpha_{20} \sin(\delta_2 - \delta_1) \cos \vartheta (3 \cos^2 \vartheta - 1) \\ &\quad + 2\alpha_{11}\alpha_{21} \sin(\delta_2 - \delta_1) \cos \vartheta \sin^2 \vartheta. \end{aligned} \quad (9)$$

Note that all the angular functions that appear in Eq. (4) for the irreducible representation  $a''$  are also present here. The

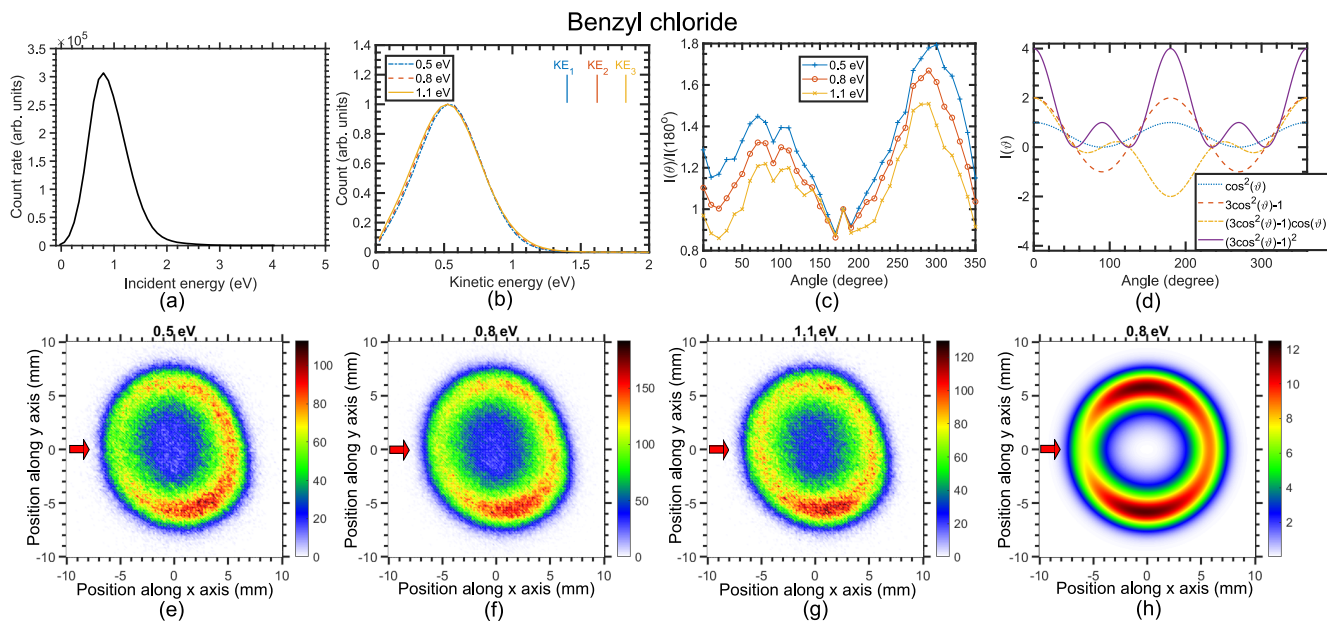


FIG. 4. The results for benzyl chloride. (a) The  $\text{Cl}^-$  ion yield as a function of the incident electron energy. (b) The kinetic energy distributions of  $\text{Cl}^-$  for three different incident energies. (c) The angular distribution of the  $\text{Cl}^-$  ions for these energies. (d) Angular terms from Eq. (9) (which did not appear in Fig. 1). (e),(f),(g) The velocity map images of  $\text{Cl}^-$  (central time slices) at three different incident energies. The incident electron beam is depicted by red arrows. (h) Simulated image using the experimental KER at the incident energy of 0.9 eV and the angular distribution described in the text.

elements of Eq. (9) that do not contribute to the irreducible representation  $a'$  [Fig. 1(d)] are plotted in Fig. 4(d).

The  $s$ -wave itself does not introduce any nontrivial angular character to the ion distribution. For this, it is necessary to assume in Eq. (1) at least the partial waves  $s$  and  $p$ . The forward-backward asymmetry of the VMI also requires including the partial wave  $d$  [see the term in Eq. (9) involving the product  $\alpha_{10}\alpha_{20}$ ].

The number of independent parameters  $\alpha_{lm}$  and  $\delta_l$  in this model based on the three lowest partial waves provides sufficient flexibility to qualitatively reproduce the observed angular structures. In fact, it is enough to choose four of them, including the mixing term  $\cos\vartheta(3\cos^2\vartheta - 1)$ , and to consider the other zero. Figure 4(h) shows the hypothetical image obtained with the optimized coefficients  $\alpha_{10} = 0.897$ ,  $\alpha_{11} = 1.083$ ,  $\alpha_{20} = 0.02$ , and  $|\delta_2 - \delta_1| = \pi/2$ . Such estimates of the contributions reproduce all the major features of the experimental distribution.

## V. CONCLUSIONS

In conclusion, we have measured velocity map images of  $\text{Cl}^-$  fragments resulting from DEA to four unsaturated chloro-substituted hydrocarbons. The choice of these compounds was inspired by the problem of the  $\pi^*$ - $\sigma^*$  mixing. In the pairs vinyl versus allyl chloride and chlorobenzene versus benzyl chloride, a similar dynamical situation arises: in the former, the dissociation can proceed only upon out-of-plane distortion of the transient anion, while in the latter, the C-Cl bond can be directly cleaved without any additional distortion. Our goal was to find out what are the imprints of this situation in the

angular distribution of ejected  $\text{Cl}^-$  fragments with respect to the direction of the incident electron beam.

All four molecules show distinctly different fragment angular distributions. Vinyl chloride shows a propensity for the perpendicular ejection of fragments. Taking into account only the  $a'$  ( $\pi^*$ ) resonance and the (unphysical) C-Cl bond stretch in planar geometry, the angular distribution of fragments resulting from the  $p$ -wave (the lowest allowed partial wave) would go as  $\sin^2\vartheta$ . This is surprisingly close to the observed distribution, which hints at only a very small out-of-plane deviation of the C-Cl bond during the dissociation. A comparison with another prototype system for the  $\pi^*$ - $\sigma^*$  coupling, acetylene  $\text{C}_2\text{H}_2$ , might be instructive at this point. There, the formation of the  $\pi^*$  resonance leads to a  $\text{C}_2\text{H}^- + \text{H}$  fragmentation channel, which cannot proceed in the linear geometry. Fogle *et al.* [41] found out that in order to reproduce the experimental angular distribution, they had to assume bending of the C-H bond by more than  $25^\circ$ . This is in strong contrast with the presently observed situation in vinyl chloride.

In allyl chloride, the parallel ejection of  $\text{Cl}^-$  fragments can be explained by direct dissociation of the  $\sigma^*(\text{C-Cl})$  state, yielding a  $\cos^2\vartheta$  distribution. In the first pair of target molecules, vinyl and allyl chloride, we thus do not observe any mixing of the  $\pi^*$  and  $\sigma^*$  symmetries. One molecule can be fully explained with the former, another with the latter. The situation is different in the second pair of molecules. Even though the analysis in chlorobenzene is complicated by the small kinetic energy release of the  $\text{Cl}^-$  fragment, the images clearly do not correspond to dissociation from the nondistorted  $b_1(\pi^*)$  resonance. This would yield fragments emitted in the perpendicular direction; the weakly prolate

shape of the experimental images suggests the presence of a parallel component ( $\cos^2 \vartheta$ ), a sign of the  $\sigma^*(\text{C-Cl})$  contribution. Finally, in benzyl chloride we observe a quite complex angular distribution that cannot be explained by treating only the isolated C-Cl bond (as it worked in allyl chloride). The relatively high partial wave  $l = 2$  has to be taken into account in order to explain the observed forward-backward asymmetry. Interestingly, benzyl chloride is the only target molecule

where the inclusion of such high partial waves was needed to explain the experimental observations.

#### ACKNOWLEDGMENT

This work is part of the Project No. 20-11460S of the Czech Science Foundation.

- 
- [1] I. I. Fabrikant, S. Eden, N. J. Mason, and J. Fedor, *Adv. At. Mol. Opt. Phys.* **66**, 545 (2017).
- [2] R. Janečková, O. May, A. R. Milosavljević, and J. Fedor, *Int. J. Mass Spectrom.* **365-366**, 163 (2014).
- [3] D. D. Clarke and C. A. Coulson, *J. Chem. Soc. A* 169 (1969).
- [4] A. Modelli and M. Venuti, *J. Phys. Chem. A* **105**, 5836 (2001).
- [5] T. Skalický, C. Chollet, N. Pasquier, and M. Allan, *Phys. Chem. Chem. Phys.* **4**, 3583 (2002).
- [6] K. Stricklett, S. Chu, and P. Burrow, *Chem. Phys. Lett.* **131**, 279 (1986).
- [7] A. Modelli, *Phys. Chem. Chem. Phys.* **5**, 2923 (2003).
- [8] N. L. Asfandiarov, V. S. Falko, A. I. Fokin, O. G. Khvostenko, G. S. Lomakin, V. G. Lukin, and E. Nafikova, *Rapid Commun. Mass Spectrom.* **14**, 274 (2000).
- [9] W. E. Wentworth, R. S. Becker, and R. Tung, *J. Phys. Chem.* **71**, 1652 (1967).
- [10] H. Shimamori, T. Sunagawa, Y. Ogawa, and Y. Tatsumi, *Chem. Phys. Lett.* **232**, 115 (1995).
- [11] Z. L. Petrović, W. C. Wang, and L. C. Lee, *J. Chem. Phys.* **90**, 3145 (1989).
- [12] A. S. Barbosa, M. T. d. N. Varella, S. v. A. Sanchez, J. a. Ameixa, F. Blanco, G. Garcia, P. Limão-Vieira, F. Ferreira da Silva, and M. H. F. Bettiga, *J. Chem. Phys.* **145**, 084311 (2016).
- [13] S. T. Chourou and A. E. Orel, *Phys. Rev. A* **77**, 042709 (2008).
- [14] O. May, J. Fedor, and M. Allan, *Phys. Rev. A* **80**, 012706 (2009).
- [15] O. May, D. Kubala, and M. Allan, *Phys. Rev. A* **82**, 010701(R) (2010).
- [16] S. T. Chourou and A. E. Orel, *Phys. Rev. A* **83**, 032709 (2011).
- [17] T. N. Rescigno, C. S. Trevisan, and A. E. Orel, *Phys. Rev. Lett.* **96**, 213201 (2006).
- [18] G. A. Gallup, P. D. Burrow, and I. I. Fabrikant, *Phys. Rev. A* **79**, 042701 (2009).
- [19] R. Janečková, D. Kubala, O. May, J. Fedor, and M. Allan, *Phys. Rev. Lett.* **111**, 203201 (2013).
- [20] T. P. R. Kumar, J. Kočíšek, K. Bravaya, and J. Fedor, *Phys. Chem. Chem. Phys.* **22**, 518 (2020).
- [21] M. Zawadzki, Čížek, K. Houfek, R. Čurík, M. Ferus, S. Civiš, J. Kočíšek, and J. Fedor, *Phys. Rev. Lett.* **121**, 143402 (2018).
- [22] D. Nandi, V. S. Prabhudesai, E. Krishnakumar, and A. Chatterjee, *Rev. Sci. Instrum.* **76**, 053107 (2005).
- [23] M. Ranković, P. Nag, M. Zawadzki, L. Ballauf, J. Žabka, M. Poláček, J. Kočíšek, and J. Fedor, *Phys. Rev. A* **98**, 052708 (2018).
- [24] A. T. J. B. Eppink and D. H. Parker, *Rev. Sci. Instrum.* **68**, 3477 (1997).
- [25] M. Ashfold, N. Nahler, A. Orr-Ewing, O. Vieuxmaire, R. Toomes, T. Kitsopoulos, I. Anton-Garcia, D. Chestakov, S.-M. Wu, and D. Parker, *Phys. Chem. Chem. Phys.* **8**, 26 (2006).
- [26] P. Nag, M. Poláček, and J. Fedor, *Phys. Rev. A* **99**, 052705 (2019).
- [27] A. Stamatovic and G. J. Schulz, *Rev. Sci. Instrum.* **39**, 1752 (1968).
- [28] O. Jagutzki, A. Czasch, and S. Schössler, in *Advanced Photon Counting Techniques VII*, edited by M. A. Itzler, SPIE Proc. Vol. 8727 (SPIE, Bellingham, 2013).
- [29] T. F. O'Malley and H. S. Taylor, *Phys. Rev.* **176**, 207 (1968).
- [30] R. Azria, Y. L. Coat, G. Lefevre, and D. Simon, *J. Phys. B* **12**, 679 (1979).
- [31] M. Tronc, F. Fiqued-Fayard, C. Schermann, and R. I. Hall, *J. Phys. B* **10**, 305 (1977).
- [32] N. B. Ram and E. Krishnakumar, *Phys. Chem. Chem. Phys.* **13**, 13621 (2011).
- [33] K. Gope, N. Mason, E. Krishnakumar, and V. S. Prabhudesai, *Phys. Chem. Chem. Phys.* **21**, 14023 (2019).
- [34] D. Chakraborty, A. Giri, and D. Nandi, *Phys. Chem. Chem. Phys.* **21**, 21908 (2019).
- [35] M. Tinkham, *Group Theory and Quantum Mechanics* (McGraw Hill, New York, 1964).
- [36] K. D. Jordan, J. A. Michejda, and P. D. Burrow, *J. Am. Chem. Soc.* **98**, 7189 (1976).
- [37] P. Burrow, A. Modelli, N. Chiu, and K. Jordan, *Chem. Phys. Lett.* **82**, 270 (1981).
- [38] K. Graupner, S. A. Haughey, T. A. Field, C. A. Mayhew, T. H. Hoffmann, O. May, J. Fedor, M. Allan, I. I. Fabrikant, E. Illenberger *et al.*, *J. Phys. Chem. A* **114**, 147 (2010).
- [39] J. K. Olthoff, J. A. Tossell, and J. H. Moore, *J. Chem. Phys.* **83**, 5627 (1985).
- [40] R. Kaufel, E. Illenberger, and H. Baumgärtel, *Chem. Phys. Lett.* **106**, 342 (1984).
- [41] M. Fogle, D. J. Haxton, A. L. Landers, A. E. Orel, and T. N. Rescigno, *Phys. Rev. A* **90**, 042712 (2014).